JOURNAL OF PLANKTON RESEARCH | VOLUME 34 | NUMBER 9 | PAGES 778–789 | 2012

Sharp gradients in phytoplankton community structure across a frontal zone in the California Current Ecosystem

ANDREW G. TAYLOR[1,*], RALF GOERICKE[1], MICHAEL R. LANDRY[1], KAREN E. SELPH[2], DANIEL A. WICK[1] AND MEGAN J. ROADMAN[1]

[1]SCRIPPS INSTITUTION OF OCEANOGRAPHY, 9500 GILMAN DR., LA JOLLA, CA 92093-0227, USA AND [2]DEPARTMENT OF OCEANOGRAPHY, UNIVERSITY OF HAWAII AT MANOA, HONOLULU, HI 96822, USA

*CORRESPONDING AUTHOR: agtaylor@ucsd.edu

Received November 5, 2011; accepted in principle April 12, 2012; accepted for publication April 16, 2012

Corresponding editor: Zoe Finkel

Spatial variability of plankton biomass, community composition and size structure was investigated across a strong frontal transition (A-Front) in the southern California Current Ecosystem in October 2008. Depth profiles were taken across a 25-km transect of nine stations sampled semi-synoptically during one night and for 3 days following drifter arrays in the adjacent water masses. Community compositions are compared based on analyses by digital epifluorescence microscopy, flow cytometry and pigment composition by high-pressure liquid chromatography. Our results show three assemblages sharply delineated in space, with plankton at the front being compositionally distinct and biomass elevated relative to either of the adjacent water masses. Depth-averaged chlorophyll *a* (Chl *a*) varied by a factor of 2.3 (0.35–0.81 μg Chl *a* L^{-1}) and autotrophic carbon (AC) varied almost 3-fold (13.6–35.4 μg C L^{-1}) across the front. One of the most striking features was a sharp gradient in the distribution of *Prochlorococcus* (PRO) and *Synechococcus* (SYN), with PRO located in the warmer oligotrophic waters on the south side of the front and SYN located in the cooler mesotrophic waters to the north. Both PRO and SYN had local biomass minima directly at the front. The peak in phytoplankton biomass at the front was dominated by large (>20 μm) diatom cells, comprising 71% of the total community biomass. In contrast to previous studies of frontal features in the southern California Current, our study of the A-Front shows strong frontal enhancement of phytoplankton biomass and a shift of phytoplankton size structure towards larger cells.

KEYWORDS: front system; epifluorescence microscopy; microbial community; biomass; size structure; HPLC; A-Front

INTRODUCTION

Sharp gradients in physicochemical properties and currents at ocean fronts are known to alter the composition and structure of plankton communities, often resulting in zones of enhanced primary production and biomass (Boucher *et al.*, 1987; Hood *et al.*, 1991; Franks, 1992a,

doi:10.1093/plankt/fbs036, available online at www.plankt.oxfordjournals.org. Advance Access publication May 24, 2012

b; Claustre *et al.*, 1994; Kemp *et al.*, 2006). Similar patterns of biological response have been found for frontal features associated with tides, shelf breaks, upwelling and geostrophic currents in varying geographic locations (Pingree *et al.*, 1978; Holligan, 1981; Houghton and Marra, 1983; Traganza *et al.*, 1987; Fiala *et al.*, 1994). Even within regions, however, results can be variable. Based on two cruises sampling across a prominent front in the southern California Current off Ensenada, Mexico, for instance, Haury *et al.* (Haury *et al.*, 1993) and Venrick (Venrick, 2000) concluded that the front did not represent a biologically distinguishable feature in terms of chlorophyll, production or phytoplankton composition. In contrast, Hood *et al.* (Hood *et al.*, 1991) found evidence of higher chlorophyll and larger phytoplankton in the vicinity of a front off northern California. Given such dissimilar findings, the nature of frontal systems and the extent to which they impact local ecology and regional productivity remain open and important questions for the California Current System, a highly productive eastern boundary region that is notably rich in mesoscale variability.

In the present study, we investigate the spatial patterns of phytoplankton and heterotrophic protists across a strong frontal feature that was sampled as part of the California Current Ecosystem (CCE), Long-Term Ecological Research (CCE-LTER) program in October 2008. The feature, referred to as 'A-Front' in this and accompanying papers, was located in a region of eastward flow, 150–500 km due west of San Diego, California. The main frontal feature was evident in satellite color and temperature images (Landry, Ohman *et al.*, 2012). We used a complementary suite of methods, digital epifluorescence microscopy, flow cytometry (FCM) and pigment analyses by high-pressure liquid chromatography (HPLC), to provide a comprehensive assessment of abundance, biomass, size structure and compositional changes across the front and in the adjacent water masses. Our results show three sharply delineated assemblages, with plankton at the front being compositionally distinct and biomass elevated relative to either of the adjacent water masses.

METHOD

Sampling

On CCE-LTER process cruise P0810 on the R/V Melville, we sampled a transect of nine stations spanning ~25 km across the frontal zone during the night of 24–25 October 2008. Sampling began in warm oligotrophic water to the south of the front (32.67°N, 120.56°W) at ~2100 local time and ended in cool eutrophic water to the north (32.90°N, 120.71°W) at ~0600 (Fig. 1). All sampling was completed during darkness. At each station, we deployed a CTD rosette with 10-L Niskin bottles to collect discrete water samples from seven to eight depths through the euphotic zone to a depth of 80 m. The chlorophyll fluorescence profile was observed on the downcast, and bottles were tripped "on-the-fly" on the upcast at variable depths that captured the mixed layer, the peak concentration of the subsurface chlorophyll maximum, if present, and the shoulders and breaks that defined those features. The Niskin bottles were sampled for analyses of total chlorophyll *a* (Chl *a*), phytoplankton accessory pigments by high performance liquid chromatography (HPLC), prokaryotic abundance and biomass by FCM and protistan community abundance and biomass by digital epifluorescence microscopy. In addition, we conducted similar sampling during experimental drifter studies in water masses to the north (Cycle 5; 22–24 October) and south (Cycle 6; 26–28 October) of the front (Fig. 1). For each of these experiments (described in Landry, Ohman *et al.*, 2012), we sampled the euphotic zone at eight depths at the location of the satellite-tracked, drogued drifter at around 03.00 each morning for three consecutive days.

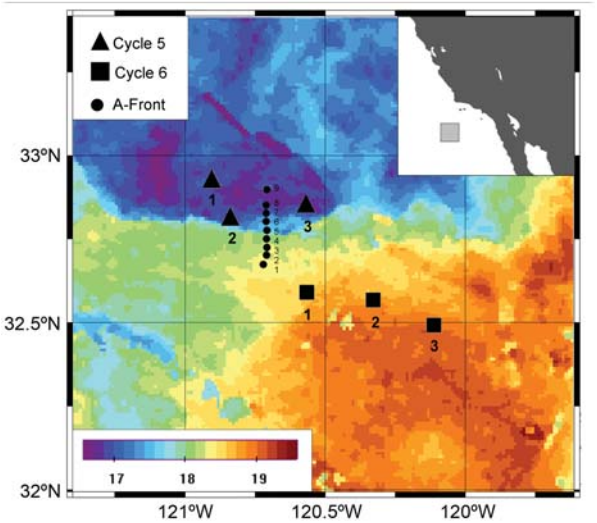

Fig. 1. Map of A-Front station locations and satellite measured sea surface temperature (SST). Circles mark the nine transect sampling stations, triangles mark the three sampling days for Cycle 5 and squares mark the three sampling days for Cycle 6. Sampling for the A-Front transect crossing was conducted from south to north in a single night. Cycle 5 and 6 samplings were conducted from west to east following drifter flows. SST is merged from MODIS Aqua and Terra satellites from the period of 22–25 October 2008. The color bar represents SST (°C).

HPLC analysis

Concentrations of lipophilic pigments, chlorophylls and carotenoids, were determined using HPLC. For HPLC analysis, 2.2- or 4.4-L samples of seawater were filtered onto Whatman GF/F filters, stored in liquid nitrogen and extracted in acetone as described by Goericke (Goericke, 2002). An internal standard (canthaxanthin) was added to the samples, which were analyzed on an Agilent 1100 series HPLC system (Agilent Technologies, Santa Clara, CA, USA) with a Waters Symmetry C8 column (3.5-μm particle size, 4.6 × 150 mm, silica, reverse-phase; Waters, Milford, MA, USA). Pigments were eluted using a gradient method with two solvents: (A) a mixture of methanol, acetonitrile and an aqueous pyridine solution (0.25 M, pH = 5) (50:25:25 v:v:v); and (B) a mixture of methanol, acetonitrile, and acetone (20:60:20 v:v:v), according to the following times and proportions (time, %A, %B): (0, 100, 0), (12, 60, 40), (36, 0, 100), (38, 0, 100) and (40, 100, 0). Contributions of chemotaxonomically defined taxa to total chlorophyll *a* [TChl *a* = chlorophyll *a* (Chl *a1*) plus divinyl-chlorophyll *a* (Chl *a2*)] were calculated as described previously (Goericke and Montoya, 1998; Goericke, 2002).

Picoplankton analysis by FCM

We enumerated pico-phytoplankton and heterotrophic bacteria from 2-mL samples preserved with 0.5% paraformaldehyde (final concentration) and flash frozen in liquid nitrogen. On shore, the samples were stored at −80°C, then thawed in batches and stained with Hoechst 34442 (1 μg mL^{-1}, final concentration) immediately prior to the analysis (Campbell and Vaulot, 1993; Monger and Landry, 1993). The analyses were conducted at the SOEST Flow Cytometry Facility (www.soest.hawaii.edu/sfcf) using a Beckman–Coulter Altra flow cytometer equipped with a Harvard Apparatus syringe pump for quantitative analyses and two argon ion lasers tuned to UV (200 mW) and 488 nm (1 W) excitation. Fluorescence signals were collected using filters for Hoechst-bound DNA, phycoerythrin and chlorophyll, all normalized to internal standards of 0.5- and 1.0-μm yellow-green (YG) polystyrene beads (Polysciences Inc., Warrington, PA, USA). Listmode data files (FCS 2.0 format) of cell fluorescence and light-scatter properties were acquired with Expo32 software (Beckman-Coulter) and used with FlowJo software (Tree Star, Inc., www.flowjo.com) to define populations of *Prochlorococcus* (PRO), *Synechococcus* (SYN), heterotrophic bacteria (H-Bact) and photosynthetic eukaryotic phytoplankton. PRO and SYN abundance estimates from FCM analyses were converted to biomass using mixed-layer estimates of 32 and 101 fg C $cell^{-1}$, respectively (Garrison *et al.*, 2000; Brown *et al.*, 2008).

Microscopical assessment of nano- and microplankton

Seawater samples were collected for analysis of the protistan eukaryote communities using advanced digital epifluorescence microscopy. Seawater samples of 500 mL were preserved according to a modified protocol of Sherr and Sherr (Sherr and Sherr, 1993), by adding 260 μL of alkaline Lugol's solution, 10 mL of buffered formalin and 500 μL of sodium thiosulfate sequentially to the samples and gently mixing between each addition. Preserved samples were allowed to sit and clear in the dark at room temperature for 1 h. They were then stained with 1 mL of proflavin (0.33% w/v) and stored in the dark for an additional hour. Just prior to filtering, the samples were stained with 1 mL of DAPI (0.01 mg mL^{-1}). A 50-mL aliquot (small volume, SV) of the sample was filtered onto a 25-mm 0.8-μm pore size black polycarbonate filter, and the remaining 450 mL aliquot (large volume, LV) was filtered onto a 25-mm 8.0-μm pore size black polycarbonate filter. A 10-μm nylon backing filter was used under all polycarbonate filters to promote even cell distribution, and all filtering was done under a gentle vacuum (<100 mm Hg). Each filter was then mounted onto glass slides using immersion oil and a No. 2 cover slip.

Slides were digitally imaged using a Zeiss Axiovert 200 M inverted compound microscope, equipped for epifluorescence microscopy and driven by Zeiss Axiovision software. The stage, filter set and focus drive were motorized to allow for automated image acquisition. Digital images were acquired with a Zeiss AxioCam HRc color CCD digital camera. Exposure times for each image were automatically determined by the software in order to avoid over exposure. SV samples (50 mL aliquots) were viewed at ×630 magnification and LV samples (450 mL aliquots) were viewed at ×200 magnification. A minimum of 20 random positions were imaged for each slide, with each position consisting of three to four fluorescent channels: Chl *a*, DAPI, FITC (SV and LV samples) and phycoerythrin (SV samples only). The separate channels were combined to form one composite 24-bit RGB image for each position.

The resulting images were processed and analyzed using ImagePro software to semi-automate the enumeration of

eukaryotic cells larger than 1.5 μm in length. Whenever possible, >300 cells were counted for each slide. Using a VBA script within the ImagePro software, a series of pre-processing steps were performed using the green channel, which corresponds to the fluorescence of proflavin staining of cell protein. The green channel was first extracted as an 8-bit gray scale image from the original 24-bit RGB image. A fast Fourier transform was applied to remove background noise, followed by the application of a Laplace filter to improve the definition of the cell edge and to minimize the halo effect common in epifluorescent images. Images that were out of focus or of poor quality were discarded. Cells were automatically segmented from the background and outlined, and the outlines are reapplied to the original 24-bit RGB image. User interaction was then required to check each image, split connected cells, outline cells that did not auto-segment from the background and delete artifacts and detritus that the software had incorrectly outlined.

Each cell was manually identified and grouped into seven plankton functional groups: diatoms, prymnesiophytes, autotrophic flagellates, heterotrophic flagellates, autotrophic dinoflagellates, heterotrophic dinoflagellates and ciliates. Autotrophic plankton was classified based on the presence of chlorophyll *a*, which autofluorences red under blue light excitation. Cells were also grouped into three size categories (Pico, <2 μm; Nano, 2–20 μm; Micro, 20–200 μm) based on the length of their longest axis. The size class for autotrophic picophytoplankton (A-Pico) also includes PRO and SYN cells measured by FCM. Biovolumes (BV; μm^3) were calculated from the length (L) and width (W) measurements of each cell using the geometric formula of a prolate sphere (BV = 0.524 LWH). For the height of cells (H), which was unmeasured, we used H = W for diatoms and H = 0.5 W for flagellates (Taylor *et al.*, 2011). Biomass was calculated as carbon (C; pg $cell^{-1}$) using the equations of Menden-Deuer and Lessard (Menden-Deuer and Lessard, 2000): $C = 0.288\ BV^{0.811}$ for diatoms, $C = 0.216\ BV^{0.939}$ for non-diatoms and C = 0.190 BV for ciliates.

Nutrient analysis

Samples for the analysis of nitrate, nitrite, ammonium, phosphate and silicate were collected from Niskin bottles into 45-mL plastic test tubes and stored frozen at −18°C until analysis ashore within 2 months of collection. Nutrients were analyzed by flow injection analysis at the nutrient laboratory of the University of California, Santa Barbara on a Lachat Instruments QuikChem 8000 using standard wet-chemistry methods (Gordon *et al.*, 1992).

Contour plots

Contour plots were generated using Ocean Data View (Schlitzer, 2006). AVG gridding algorithm was used for variable resolution in a rectangular grid where grid spacing varied accordingly to data density.

RESULTS

Hydrography and nutrients

In late October 2008, the A-Front was evident as a strong east–west orientated surface feature at ~32.8°N, 121.8°W in satellite color and temperature images (Landry, Ohman *et al.*, 2012). The 16°C isotherm clearly marked the location of the front at the surface. Several underway transects across the front conducted prior to the nighttime sampling showed that its location wandered slightly during the day (Ohman *et al.*, 2012), perhaps reflecting tides or current undulations along its length. Observed surface currents in the vicinity of the front (upper 60 m) flowed west-to-east at speeds of 20–30 cm s^{-1} (Li *et al.*, 2012). Currents north of the front were weaker, flowing in a northeasterly direction. Below the surface, the front was evident to 80-m depth, clearly delimited by the 33.4 isohaline (Landry, Ohman *et al.*, 2012). Water masses in the upper 100 m to the north of the front were saline and cool, as typical for the northern coastal area where upwelling occurs. South of the front, low salinity water of the California Current was evident at a depth of 60 m, subducted below higher salinity water, a mixture of the California Current and central Pacific subtropical waters that flow into the Southern California Bight from the south during summer. At the front (Stations 4 and 5), isotherms and isohalines broadened from 20 to 60 m, likely reflecting shear-induced mixing.

The depth where concentrations of nitrate reach values of 1 μM, i.e. the nitracline, increased gradually from 40 m south of the front to 30 m north of the front (Fig. 2). At the front, concentrations of nitrate were slightly elevated in the upper 30 m. Phosphate followed the distribution of nitrate (data not shown). Concentrations of ammonium in the upper 25 m (0.2–0.4 μM) did not vary systematically across the front. A subsurface ammonium maximum was observed at ~35 m at the front and to the north. The average molar carbon to nitrogen ratio of particulate matter in

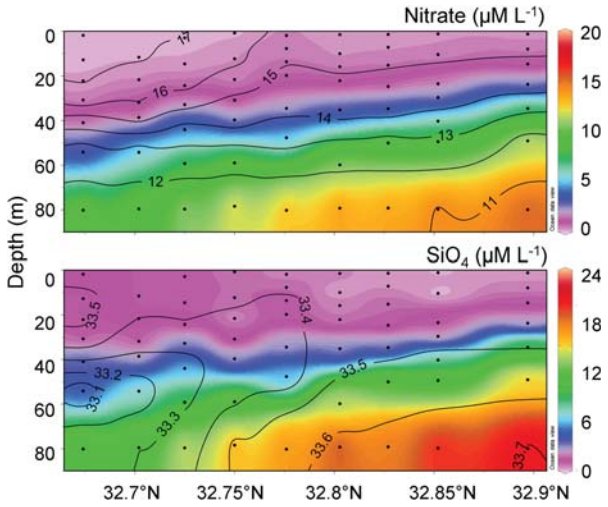

Fig. 2. Distributions of nitrate and SiO_4 ($\mu M\ L^{-1}$) across A-Front. For the nitrate panel, black lines are contours of isotherms (°C) and for the SiO_4 panel black lines are contours of isohalines (PSU).

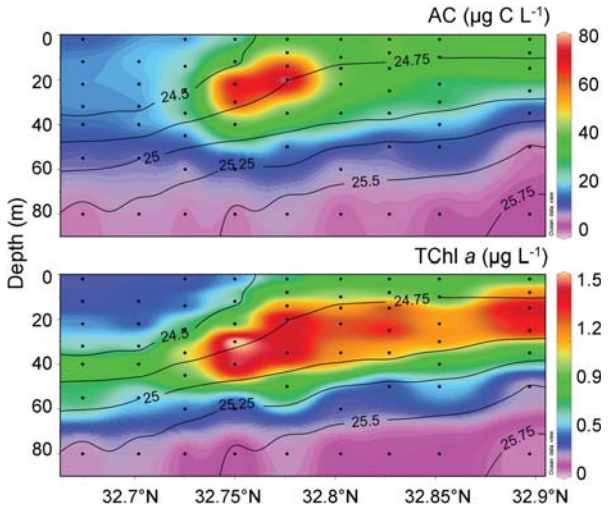

Fig. 3. Distributions of total chlorophyll *a* (TChl *a* = μg Chl *a* L^{-1}) and total autotrophic carbon (AC = μg C L^{-1}) across A-Front. Black lines are contours of density surfaces (kg m^{-3}).

the upper 45 m south of the front ranged from 6.5 to 7.7 and was substantially lower at the front (4.8) and to the north (5.3–6.5).

Chlorophyll *a* and autotrophic biomass

Chlorophyll *a* distribution shows a strong subsurface maximum across the frontal transect, located between the 24.75 and 25.00 isopycnals (Fig. 3). The depth of this maximum shoaled from ~40 m on the southern side of the front to ~20 m on the northern side. Averaged over the upper 80 m of the water column at each station, Chl *a* concentrations varied from 0.35 to 0.81 μg Chl *a* L^{-1}, with a grand mean of 0.57 ± 0.15 μg Chl *a* L^{-1} for the transect (Table I). The highest depth-averaged Chl *a* values (0.81 μg Chl *a* L^{-1}) were found at the front Stations 4 and 5, while mean concentrations to the south and north were 0.4 and 0.6 μg Chl *a* L^{-1}, respectively. The 3-day depth-averaged Chl *a* concentration for Cycle 5 north of the front (0.86 ± 0.13 μg Chl *a* L^{-1}) was three times higher than Cycle 6 south of the front (0.28 ± 0.01 μg Chl *a* L^{-1}) and about the same as at the front (0.81 μg Chl *a* L^{-1}). The highest Chl *a* concentrations observed were on the first and second days of cycle 5 (Table I).

Following the general distribution pattern for Chl *a*, lower values of autotrophic carbon (AC), calculated from FCM and microscopy, were located south of the front and higher values to the north. The depth of the AC maximum also shoaled from south to north, although slightly shallower than the subsurface Chl *a* maximum due to pigment photoadaptation (i.e. increasing cellular Chl *a* content with depth) (Fig. 3). AC distribution differs from Chl *a* in the magnitude of subsurface enhancement at the front, as opposed to the more uniform Chl *a* depth profiles from the front to the most northern station sampled. That is, while both measurements showed local enhancements of phytoplankton standing stock at the front, AC more strongly defined the subsurface biomass maximum (20–40 m) at the front relative to the adjacent water masses. Depth-averaged AC varied almost 3-fold, from 13.6 to 35.4 μg C L^{-1}, across the front, with a mean of 21.4 ± 8.0 μg C L^{-1} (Table I). The highest values were found directly at the front (34.3 ± 1.5 μg C L^{-1}) compared with northern and southern station averages of 20.1 ± 2.9 and 14.6 ± 1.0 and μg C L^{-1}, respectively. Similarly, the mean AC concentration during the northern Cycle 5 experiments (22.8 ± 3.7 μg C L^{-1}) was substantially higher than during Cycle 6 (9.7 ± 0.4 μg C L^{-1}), but less than at the front.

Biomass estimates of phototrophic and heterotrophic prokaryotes

Biomass estimates of the phototrophic bacteria PRO and SYN, enumerated by FCM, showed very strong but opposing gradients across the frontal system (Fig. 4). PRO biomass was highest on the southern, oligotrophic side (mean depth-averaged station biomass 2.6 ± 0.8 μg C L^{-1}) and was almost zero on the northern, mesotrophic side (Table I). The distribution of Chl *a2*, a unique biomarker for PRO, followed the pattern for PRO cell counts, except that the concentration maximum was deeper, reflecting changing carbon to

Table I: Mean phytoplankton abundance and biomass estimates for the A-Front study

				Abundance (cells mL^{-1})			Biomass (μg C L^{-1})							
		Lat (°N)	Lon (°W)	A-Pico	A-Nano	A-Micro	PRO	SYN	A-Pico	A-Nano	A-Micro	Chl	AC	AC:Chl
Mean station auto														
Cycle 6 (day)	1	32.60	120.56	200	2000	15	2.1	0.8	0.06	4.2	2.3	0.27	9.5	35
	2	32.57	120.33	190	2100	12	3.2	0.7	0.06	4.0	1.6	0.29	9.6	33
	3	32.49	120.11	80	1600	10	3.2	1.0	0.02	4.6	1.3	0.28	10.1	36
A-Front (stn)	1	32.67	120.72	350	3000	10	3.5	1.8	0.11	5.9	2.4	0.39	13.6	35
	2	32.70	120.71	380	4000	20	2.1	1.7	0.12	7.9	2.6	0.35	14.4	41
	3	32.73	120.71	450	3500	20	2.2	1.9	0.14	7.7	3.6	0.44	15.6	35
	4	32.75	120.71	230	2500	100	0.6	0.9	0.07	18.7	13.0	0.68	33.3	49
	5	32.78	120.71	220	2600	160	0.0	0.6	0.07	17.1	17.7	0.81	35.4	43
	6	32.80	120.71	100	2700	60	0.0	6.3	0.03	10.4	5.9	0.66	22.7	34
	7	32.83	120.71	170	3600	50	0.0	6.1	0.05	10.4	4.6	0.63	21.2	34
	8	32.85	120.71	180	2800	40	0.0	7.2	0.05	7.7	5.7	0.55	20.8	38
	9	32.90	120.71	50	1800	30	0.1	4.2	0.02	7.1	4.5	0.57	15.9	28
Cycle 5 (day)	1	32.92	120.90	120	2500	80	0	4.2	0.04	11.6	8.3	0.98	24.1	25
	2	32.82	120.84	120	2100	100	0	2.6	0.04	12.6	10.3	0.88	25.6	29
	3	32.85	120.57	90	1600	70	0	2.1	0.03	8.9	7.5	0.72	18.6	26

All estimates were first integrated, and then averaged for the upper 80 m at each station. Categories are: autotrophic prokaryotes [PRO and SYN] from FCM analyses, and autotrophic eukaryotes by size class [A-Pico (0.2–2 μm), A-Nano (2–20 μm) and A-Micro (20–200 μm)] from epifluorence microscopy. Mean values of total chlorophyll *a* (Chl), total autotrophic biomass (AC = sum of prokaryotes and eukaryotes) and autotrophic carbon to chlorophyll *a* ratio (AC:Chl) are also given. Units are cells mL^{-1} for abundance, μg C L^{-1} for biomass and μg Chl *a* L^{-1} for chlorophyll.

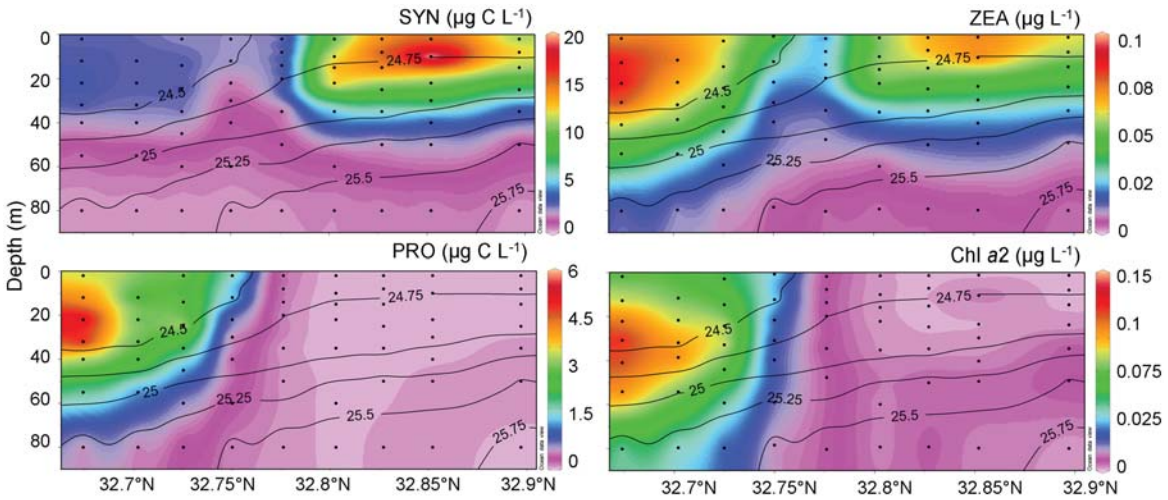

Fig. 4. Distributions of phototrophic prokaryotes PRO and SYN across A-Front, as determined by FCM. Units are μg C L^{-1}, and note that scales are different for each plot. Distributions of the PRO taxon-specific marker pigment divinyl chlorophyll *a* (Chl *a2*) and zeaxanthin (ZEA) which is specific to both SYN and PRO, as determined by HPLC. Units are μg pigment L^{-1}, and note that scales are different for each plot. Black lines are contours of density surfaces (kg m^{-3}).

Chl *a2* ratios due to photoadaptation. In contrast to PRO, the SYN biomass was highest on the northern side (mean depth-averaged station biomass 6.0 ± 1.3 μg C L^{-1}) and diminished greatly south of the front (Table I). Similarly, PRO biomass was undetectable in the mesotrophic waters of Cycle 5, while SYN averaged 3.0 ± 1.1 μg C L^{-1}. During Cycle 6, PRO biomass averaged 2.8 ± 0.66 μg C L^{-1} while SYN was 0.9 ± 0.16 μg C L^{-1}.

Another interesting feature of the front transect is that both PRO and SYN had local biomass minima directly at the front: for Stations 4 and 5, PRO and SYN averaged 0.3 and 0.8 μg C L^{-1}, respectively (Table I). This result is confirmed by the distribution of zeaxanthin, a non-photosynthetically active pigment marker for cyanobacteria, which also showed a local minimum at the front. For the most part, the bulk of PRO and SYN cells and pigments was contained within the upper 50 m depth of southern waters and the upper 30 m in the north.

Heterotrophic bacteria (H-Bact) also showed a strong gradient across the frontal system with highest mean 0–

Table II: Mean abundance and biomass estimates of heterotrophs for the A-Front study

			Abundance (cells mL^{-1})			Biomass (μg C L^{-1})				
	Lat (°N)	Lon (°W)	H-Pico	H-Nano	H-Micro	H-Bact	H-Pico	H-Nano	H-Micro	HC
Cycle 6 (day)										
1	32.60	120.56	50	800	2	6.1	0.02	1.9	1.0	2.9
2	32.57	120.33	70	900	1	6.4	0.02	1.7	0.3	2.1
3	32.49	120.11	10	500	2	8.2	0.00	2.0	1.0	3.0
A-Front (stn)										
1	32.67	120.72	90	1200	1	8.6	0.03	1.8	0.4	2.3
2	32.70	120.71	110	1500	1	7.7	0.03	2.6	0.3	3.0
3	32.73	120.71	90	1300	2	7.9	0.03	2.9	1.2	4.1
4	32.75	120.71	80	1100	2	8.5	0.02	2.4	1.2	3.6
5	32.78	120.71	40	900	3	9.3	0.01	2.6	1.0	3.6
6	32.80	120.71	110	1800	3	14.9	0.03	4.2	1.4	5.6
7	32.83	120.71	100	1500	3	13.6	0.03	4.4	1.3	5.7
8	32.85	120.71	60	1200	3	17.1	0.02	3.1	2.0	5.2
9	32.90	120.71	50	900	4	13.3	0.01	3.9	1.4	5.3
Cycle 5 (day)										
1	32.92	120.90	90	1400	2	19.7	0.03	3.4	1.2	4.7
2	32.82	120.84	60	1300	3	13.5	0.02	3.4	1.4	4.8
3	32.85	120.57	60	1000	3	12.5	0.02	2.8	1.8	4.7

All estimates were first integrated, and then averaged for the upper 80 m at each station. Categories are: heterotrophic bacteria (H-Bact) from FCM analyses, and heterotrophic eukaryote by size class. H-Pico (0.2–2 μm), H-Nano (2–20 μm) and H-Micro (20–200 μm) from epifluorescence microscopy. Heterotrophic carbon (HC) is the sum for all eukaryote size classes (i.e. protistan grazers), excluding H-Bact. Units are cells mL^{-1} for abundance, and μg C L^{-1} for biomass.

80 m biomass concentrations on the northern side of the front (15 ± 1.7 μg C L^{-1}) and lower values to the south (8.1 ± 0.4 μg C L^{-1}) (Table II). H-Bact biomass averaged 15 ± 3.9 μg C L^{-1} during Cycle 5 and 6.9 ± 1.3 μg C L^{-1} during Cycle 6.

Biomass distributions of heterotrophic protists

Depth-averaged station estimates for heterotrophic protist biomass (H-Protist) varied by more than 2-fold across the front (from 2.3 to 5.5 μg C L^{-1}), with a mean value of 4.1 ± 1.2 μg C L^{-1} (Table II). Station estimates were lowest on the south side of the front and increased towards the north, with the highest biomass at Station 7. Component assemblages of H-Flag and H-Dino ranged from 0.7 to 2.3 μg C L^{-1} (mean 1.2 ± 0.56 μg C L^{-1}) and from 1.6 to 4.1 μg C L^{-1} (mean 3.0 ± 0.8 μg C L^{-1}), respectively. Nano-sized heterotrophic flagellates (H-Nano, 2–20 μm) comprised the majority (mean = 76%) of the biomass, while H-Pico (<2 μm) and H-Micro (20–200 μm) cells accounted for 0.6 and 27%, respectively (Table II). H-Nano contributed 68% to H-Protist biomass in Cycle 5 and 71% in Cycle 6, while H-Micro contributed 31% in Cycle 5 and 29% in Cycle 6.

Biomass of ciliated protists is likely underestimated in our epifluorescence microscopy counts (Taylor *et al.*, 2011), and is therefore not included in the estimates above for heterotrophic flagellates. Nevertheless, the relative concentrations of ciliates that we did enumerate were found to be highest directly on the front (Table III).

Distributions of eukaryotic autotroph groups

Based on microscopy, diatoms dominated the maximum in autotroph carbon (AC) at front Stations 4 and 5, contributing 78–86% of AC at the 20–40 m depths of their maximum concentrations (Fig. 5). The distribution of fucoxanthin, a pigment found primarily in diatoms, strongly supports the subsurface maximum of diatom biomass at the front. North of the front, the diatom contribution to total biomass decreased, ranging from 34% of AC in the subsurface Chl maximum to <13% in the mixed layer.

Dinoflagellates biomass showed an enriched area extending north from front Stations 5–7, but the highest biomass was at the surface north of the front (Station 7; Fig. 5). Distribution of the pigment-marker peridinin diverged markedly from microscopically derived autotrophic dinoflagellate (A-Dino) carbon, reflecting changing pigment-biomass ratios as a function of depth as well as the lack of peridinin in some dinoflagellate species. Prymnesiophyte biomass was highest primarily in near-surface waters north of the front, but their associated pigment marker, hexfucoxanthin,

Table III: Station values of euphotic-zone integrated biomass (0–80 m) for all enumerated plankton taxa: PRO, SYN, A-Dino, diatoms, autotrophic flagellates (A-Flag), prymnesiophytes (Prym), heterotrophic prokaryotes (H-Bact), heterotrophic dinoflagellates (H-Dino), heterotrophic flagellates (H-Flag) and ciliates (CIL)

			Depth integrated biomass (mg C m^{-2})												
	Lat (°N)	Lon (°W)	PRO	SYN	A-Dino	Diatom	A-Flag	Prym	H-Bact	H-Dino	H-Flag	CIL	AC	HC	Biomass
Cycle 6 (day)															
1	32.60	120.56	170	70	150	120	100	150	500	160	80	0	760	240	1000
2	32.57	120.33	260	60	130	90	120	110	500	80	80	0	770	170	940
3	32.49	120.11	260	80	130	50	160	130	700	160	80	0	810	240	1050
A-Front (stn)															
1	32.67	120.72	280	140	370	40	150	110	700	130	50	0	1090	180	1270
2	32.70	120.71	170	130	430	110	130	180	600	170	60	0	1150	240	1390
3	32.73	120.71	170	150	410	180	150	190	600	240	70	20	1250	310	1560
4	32.75	120.71	40	70	380	1900	120	150	700	200	60	30	2660	260	2920
5	32.78	120.71	3	50	460	2000	150	160	700	220	70	60	2830	290	3120
6	32.80	120.71	1	500	380	580	180	160	1200	260	150	40	1810	410	2220
7	32.83	120.71	2	490	420	340	240	210	1100	260	180	10	1700	440	2140
8	32.85	120.71	4	580	310	450	150	160	1400	330	90	0	1660	420	2080
9	32.90	120.71	5	340	360	290	120	170	1100	310	100	20	1280	410	1690
Cycle 5 (day)															
1	32.92	120.90	3	330	310	780	370	120	1600	250	120	0	1930	380	2310
2	32.82	120.84	3	210	360	1100	290	120	1100	240	140	0	2050	380	2430
3	32.85	120.57	2	160	230	780	220	90	1000	250	120	0	1480	370	1850

Total autotrophic carbon (AC) includes both prokaryotes and eukaryotes. Total heterotrophic carbon (HC) includes only eukaryotes. Total biomass = AC + HC, exclusive of H-Bact. Units are mg C m^{-2}.

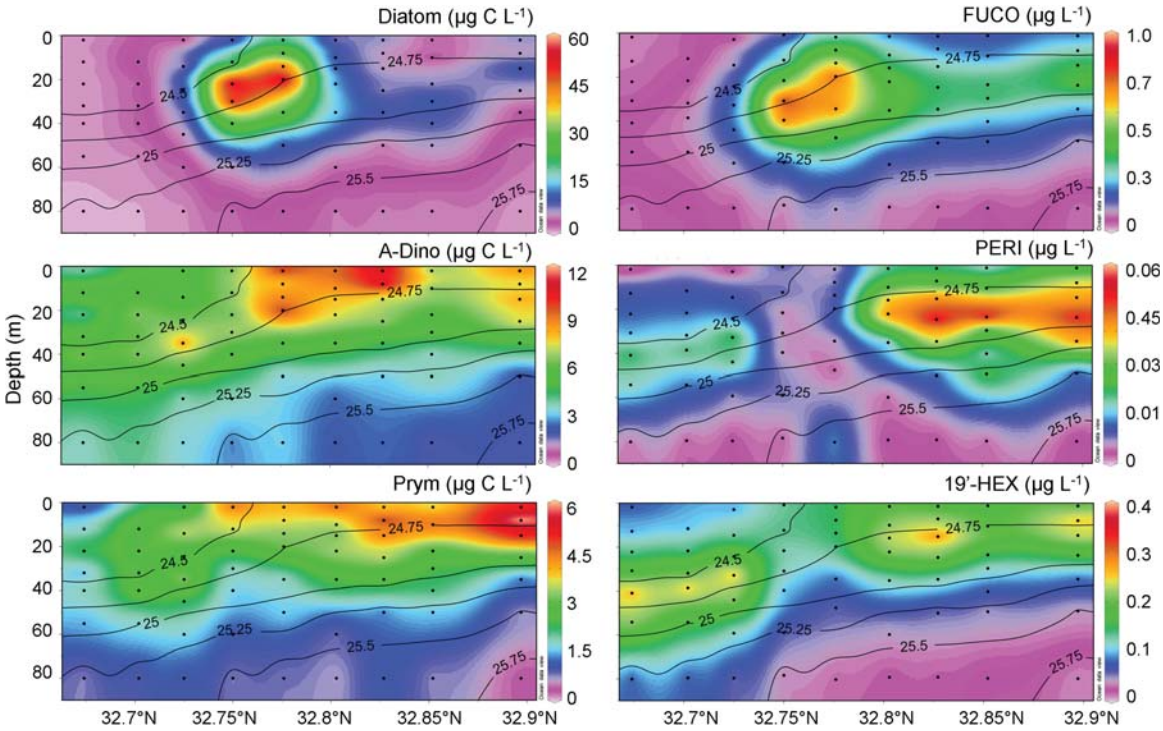

Fig. 5. Distributions of select phytoplankton marker pigments and phytoplankton functional groups across A-Front. Fucoxanthin (FUCO), Peridinin (PERI), 19′-hexanoyloxyfucoxanthin (19′-HEX), as determined by HPLC; and diatom, A-Dino and prymnesiophytes (Prym), as determined by microscopy. Units are µg pigment L^{-1} and µg C L^{-1}. Note the different scales used for each plot. Black lines are contours of density surfaces (kg m^{-3}).

showed a subsurface maximum at 30–40 m south of the front.

Integrated community composition, biomass and size-structure

For the nine transect stations, depth-integrated autotrophic biomass (AC) varied 2.6-fold, ranging from 1090 to 2830 mg C m^{-2}, with a mean value of 1720 ± 640 mg C m^{-2} (Table III). The highest AC was found directly at the front (Stations 4 and 5, 2750 mg C m^{-2}), about double the mean concentration to the south and north (1420 mg C m^{-2}). Diatoms dominated the phytoplankton community at the front, with 6.8 times higher biomass (1951 ± 84 mg C m^{-2}) than the north–south station mean (286 ± 193 mg C m^{-2}) (Fig. 6A). The average euphotic-zone integrated AC biomass for Cycle 5 (1820 ± 300 mg C m^{-2}) was more than double the integrated biomass found for Cycle 6 (780 ± 28 mg C m^{-2}) (Fig. 6). For both cycles and the transect stations, all euphotic-zone integrations were done to 80 m. While the transect was sampled at night, and we do not have any light measurements for these specific stations, we do have noon cast CTD profiles from cycles 5 and 6. These CTD casts show that 80 m depth is well below the 0.1% light level.

Biomass contributions of each phototrophic group were variable across the front, but organized into three community groups (Fig. 6A); the southern community (Stations 1–3), a front community (Stations 4 and 5) and the northern community (Stations 6–9). A principal component analysis was performed using all of the phototrophic groups (PRO, SYN, diatoms, A-Dino, A-Flag and Prym), which also split the phototrophic community into these three groups (Fig. 7). The first two principal components, diatoms and SYN, accounted for 88 and 8.6% of the variance, respectively. The oligotrophic cluster was comprised of Cycle 6 and transect Stations 1–3, the front cluster was transect Stations 4 and 5 and the mesotrophic cluster was comprised of Cycle 5 and transect Stations 6–9. The southern community was dominated by autotrophic dinoflagellates (A-Dino) which made up 35% of the total community biomass, followed by PRO (18%), prymnesiophyte (Prym; 13.5%), autotrophic flagellates (AF;12%), SYN (12%) and diatoms (9.2%) (Table IV). The front community was dominated by diatoms (71.3%), followed by A-Dino (14.9%), Prym (5.8%), AF (4.9%), SYN (2.1%) and PRO (0.9%). The northern frontal community was more diverse, with SYN (29.1%), diatoms (25.3%) and A-Dino (23.2%) comprising the bulk of the biomass, followed by Prym (11.3%), AF (10.8%) and PRO (0.2%). Diatoms comprised

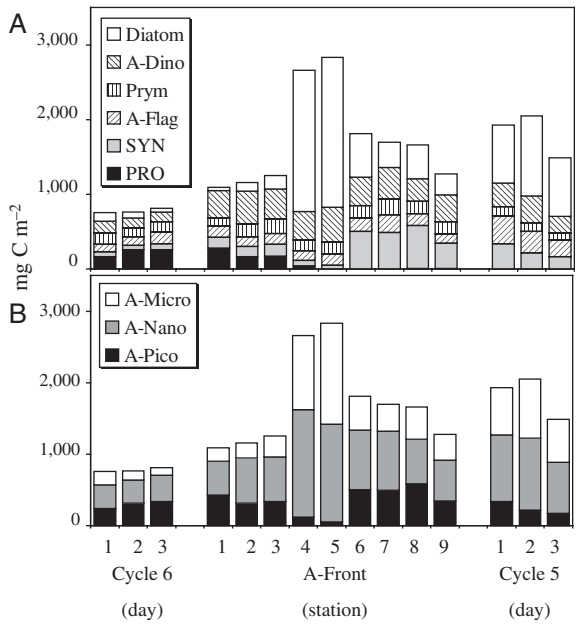

Fig. 6. (**A**) Biomass contributions of phytoplankton functional groups to total euphotic-zone integrated autotrophic community biomass: diatom, A-Dino, prymnesiophytes (Prym), autotrophic flagellates (A-Flag), SYN and PRO. (**B**) Biomass contributions of phytoplankton size classes to total euphotic-zone integrated autotrophic community biomass: A-Micro (20–200 μm), A-Nano (2–20 μm) and A-Pico (0.2–2 μm). Units are mg C m^{-2} for both plots; determined by microscopy and FCM.

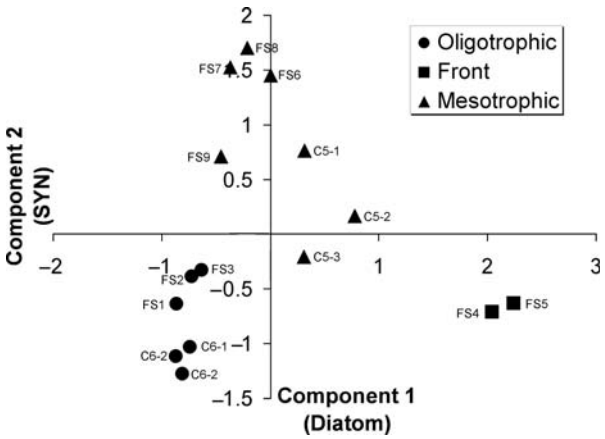

Fig. 7. Results of a principal component analysis using all of the phytoplankton groups [PRO, SYN, diatoms, A-Dino, prymnesiophytes and autotrophic flagellates]. The first two principal components, diatom and SYN, explained 88 and 8.6% of the variance, respectively. The oligotrophic cluster is Cycle 6 (C6-1, C6-2, C6-3) and transect Stations 1–3 (FS1, FS2, FS3). The front cluster is transect Stations 4–5 (FS4, FS5). The mesotrophic cluster is Cycle 5 (C5-1, C5-2, C5-3) and transect Stations 6–9 (FS6, FS7, FS8, FS9).

almost half (48.5%) of the autotrophic community biomass during the Cycle 5 experiments, followed by A-Dino (16%), A-Flag (16.3%), SYN (12.9%) and Prym

Table IV: Percentage contribution of each phytoplankton taxa and size-class to euphotic-zone integrated biomass of the autotrophic community in cycles 5 and 6, and south front (Stations 1–3), front (Stations 4-5) and north front (Stations 6–9)

	Cycle 6	Stations 1–3	Stations 4 and 5	Stations 6–9	Cycle 5
PRO	29 ± 6.7	18 ± 6.5	0.9 ± 1.1	0.2 ± 0.1	0.2 ± 0.0
SYN	9 ± 1.3	12 ± 0.7	2 ± 0.9	29 ± 3.2	13 ± 3.9
A-Dino	18 ± 2.1	35 ± 2.6	15 ± 0.9	23 ± 4.1	16 ± 1.1
Diatom	11 ± 5.0	9 ± 5.3	71 ± 0.4	25 ± 5.4	49 ± 7.0
A-Flag	16 ± 3.2	12 ± 1.6	5 ± 0.3	10 ± 2.0	16 ± 2.8
Prym	17 ± 2.5	14 ± 3.0	6 ± 0.3	11 ± 1.8	6.0 ± 0.3
A-Pico	38 ± 6	31 ± 7	3 ± 2	30 ± 3	13 ± 4
A-Nano	44 ± 2	49 ± 6	53 ± 5	45 ± 4	48 ± 1
A-Micro	18 ± 6	20 ± 3	44 ± 7	26 ± 3	38 ± 4

PRO, SYN, A-Dino, Diatom, autotrophic flagellate (A-Flag) and prymnesiophyte (Prym). Pico-autotrophs (A-Pico; 0.2-2 μm), Nano-autotrophs (A-Nano; 2–20 μm) and Micro-autotrophs (A-Micro; 20–200 μm). Data are means ± standard deviations.

(6.0%). During Cycle 6, PRO was the largest contributor (29%) to AC; A-Dino (17.9%), Prym (16.9%) and A-Flag (16.2%) contributed roughly equal shares to comprise half of the total biomass, and diatoms (11.1%) and SYN (8.9%) made up the remainder.

Phytoplankton size class distributions were very similar on the northern and southern sides of the front, with nano-sized autotrophs (2–20 μm) comprising 44 and 49% of AC, respectively, and A-Micro accounting for 26 and 20%, respectively (Fig. 6B, Table IV). Pico-autotrophs (<2 μm), primarily PRO south of the front and SYN north of the front, contributed the same fractions, 30 and 31%, respectively, to total AC. These proportions were markedly skewed to larger size classes at the front, where A-Pico, Nano and Micro contributed 3, 53 and 44% of total AC. During Cycle 5, the proportion of larger phytoplankton was higher (A-Micro = 38%) and smaller phytoplankton lower (A-Pico = 13%) than the average for the northern transect stations. For Cycle 6, the contribution of A-Micro was lower (18%) and A-Pico higher (38%) than the mean for the southern transect stations.

DISCUSSION

For this study, we used a complementary set of measurements from microscopy, FCM and HPLC pigment analysis to provide a comprehensive assessment of microbial community biomass, composition and size-structure changes across a frontal transition in the California Current System, or an Eastern Boundary Current. Overall, we observed generally good agreement between the biomass distributions of phytoplankton groups from microscopy and FCM and the patterns of diagnostic marker pigments: fucoxanthin (diatoms), 19′-hexanoyloxyfucoxanthin (prymnesiophytes), divinyl Chl *a* (PRO) and zeaxanthin (cyanobacteria) (Figs 4 and 5). While dinoflagellate biomass and peridinin values agreed reasonably well north and south of the front, this was not the case at front Station 5. This disparity suggests that the composition of dinoflagellates at the front may have included forms that lack or have substantially lower cell contents of the peridinin accessory pigment (c.f. Tangen and Björnland, 1981; Jeffrey and Wright, 2005).

One of the most striking features of our A-Front crossing was the sharp discontinuity in abundances of the phototrophic bacteria, PRO and SYN, with PRO located in the warm and oligotrophic waters to the south and SYN located in the cool and eutrophic waters to the north, and both groups showing depressed abundance directly at the front. The other major feature was the almost 7-fold increase in diatom biomass, attributed to micro-sized (>20 μm) cells at the front. Both patterns are similar to observations from upwelling and geostrophic fronts in the Alboran Sea (Claustre *et al.*, 1994; Fiala *et al.*, 1994; Reul *et al.*, 2005) and a geostropic front in the western Mediterranean Sea (Jacquet *et al.*, 2002). For the latter, Jacquet *et al.* (Jacquet *et al.*, 2002) were able to distinguish a mesotrophic system in Atlantic waters dominated by eukaryotes and SYN and a more oligotrophic system in the Mediterranean Sea waters dominated by PRO. For the former, Fiala *et al.* (Fiala *et al.*, 1994) found that Chl *a*, fucoxanthin and microscopy estimates of diatom abundance were one to two orders of magnitude higher in the frontal jet than in the surrounding waters, while pico- and nanoplankton were most abundant in the adjacent waters and consisted mostly of prymnesiophytes. At this front, the distribution of Chl *a* concentration at the depth of the chlorophyll maximum ranged from 0.2 to 2.6 μg Chl *a* L^{-1}, similar to the range that we found across the A-Front system, if we include Cycles 5 and 6 (0.47–2.0 μg Chl *a* L^{-1}). Fiala *et al.* (Fiala *et al.*, 1994) reported similar densities of >20-μm diatom cells (1–200 cells mL^{-1}) in the Chl *a* maximum of their frontal jet to what we found in our study area (10–220 cells mL^{-1}). The similarities in observations for these very different front-generating mechanisms suggest common patterns of community response to environmental perturbations at frontal transitions.

The commonalities in community changes at fronts are not so evident within the California Current System, however. For a front study off of Northern California, for example, Hood *et al.* (Hood *et al.*, 1991)

reported a significant increase in large phytoplankton on the cold eutrophic side of the water mass transition, rather than directly in the frontal jet. This observation was based on size-fractionated Chl *a*, with photomicrographs confirming qualitatively the increased abundance of chain-forming diatoms. In a study slightly to the south of our site, off of Ensenada, Mexico, Haury *et al.* and Venrick (Haury *et al.*, 1993; Venrick, 2000) concluded that the front only marked the transition of water masses, with no evidence of local enhancement of biomass or altered community composition. These differences would lead us to believe that frontal formation mechanisms or community responses to fronts are sufficiently varied to require substantial additional research to understand their differences, as well as the overall contributions of fronts to regional productivity and local ecology.

In the present study, the altered structure of the phytoplankton community observed directly at the A-Front seems to have profound impacts on many aspects of local trophic ecology. These include enhanced microbial activity (Samo *et al.*, 2012), increased suspended particulates and altered composition and biomass of mesozooplankton (Ohman *et al.*, 2012), and increased densities of acoustically estimated krill and fish (Lara Lopez *et al.*, 2012). The area of highest diatom biomass directly on the front was also the area with the highest variable fluorescence (F_v/F_m) (Chekalyuk *et al.*, 2012), a measure of the maximum quantum yield of photosynthesis that can be used as an indicator of nutrient stress. The high F_v/F_m found at the front, along with the substantial increase in large diatoms, suggests that the area was enriched with nutrients and highly productive. Along with the dramatic change in the community structure, this finding supports the hypothesis that the enhanced phytoplankton community at the front was the result of active *in situ* growth, rather than the passive accumulation of biomass in a zone of physical convergence. It is likely, however, that the assemblage observed in the frontal jet originated from upstream. As the California Current frontal jet makes its way down the coast, its community composition is affected by convergent flows and subduction from adjacent coastal surface waters (Hood *et al.*, 1991) and by nutrient intrusions and wind forcing events along the way (Franks and Walstad, 1997). How the relative contributions of local growth enhancement processes versus upstream and advective effects to community composition change across California Current frontal features is an important question for future research.

Our observations of the phytoplankton community response across A-Front also bring into question how global climate change may impact the CCE. It is thought, for example, that a warming planet could lead to enhanced thermal stratification of open-ocean waters, while at the same time intensifying winds, due to land-sea warming differences, that drive coastal upwelling (Bakun, 1990; Snyder *et al.*, 2003). Consequently, the frequency and intensity of frontal features along the along eastern boundary current regions where open-ocean and coastal upwelling waters meet might reasonably increase. Indeed, Kahru *et al.* (Kahru *et al.*, 2012) have shown increasing trends in the frequencies of thermal and chlorophyll fronts in the A-Front study area over the last decades. If enhancement of phytoplankton biomass and a community shift towards larger cells are common characteristics of such frontal features, as seen in this and other investigations, we can hypothesize that increased frontal frequency could lead to higher productivity, carbon export and food web transfer efficiency in the southern CCE.

ACKNOWLEDGEMENTS

We thank the captain and crew of the R/V Melville and all participants in the CCE-LTER process cruises.

FUNDING

The A-Front study was supported by U. S. National Science Foundation grants OCE 04-17616 and 10-26607 for the CCE LTER Program.

REFERENCES

Bakun, A. (1990) Global climate change and intensification of coastal ocean upwelling. *Science*, **247**, 198–201.

Boucher, J., Ibanez, F. and Prieur, L. (1987) Daily and seasonal variations in the spatial distribution of zooplankton populations in relation to the physical structure in the Ligurian front. *J. Mar. Res.*, **45**, 133–173.

Brown, S. L., Landry, M. R., Yang, E. J. *et al.* (2008) Diatoms in the desert; plankton community response to a mesoscale eddy in the subtropical North Pacific. *Deep-Sea Res. II*, **55**, 1321–1333.

Campbell, L. and Vaulot, D. (1993) Photosynthetic picoplankton community structure in the subtropical North Pacific Ocean near Hawaii (station ALOHA). *Deep-Sea Res. I*, **40**, 2043–2060.

Chekalyuk, A. M, Landry, M. R., Goericke, R. *et al.* (2012) Laser fluorescence analysis of phytoplankton across a frontal zone in the California Current Ecosystem. *J. Plankton Res.*, **34**, 761–777.

Claustre, H., Kerhervé, P., Marty, J. C. *et al.* (1994) Phytoplankton dynamics associated with a geostrophic front: ecological and biogeochemical implications. *J. Mar. Res.*, **52**, 711–742.

Fiala, M., Sournia, A., Claustre, H. *et al.* (1994) Gradients of phytoplankton abundance, composition and photosynthetic pigments across the Almeria-Oran front (SW Mediterranean Sea). *J. Mar. Syst.*, **5**, 223–233.

Franks, P. J. S. (1992a) Sink or swim: accumulation of biomass at fronts. *Mar. Ecol. Prog. Ser.*, **82**, 1–12.

Franks, P. J. S. (1992b) Phytoplankton blooms at fronts: patterns, scales and physical forcing mechanisms. *Rev. Aqua. Sci.*, **6**, 121–137.

Franks, P. J. S. and Walstad, L. J. (1997) Phytoplankton patches at fronts: a model of formation and response to wind events. *J. Mar. Res.*, **55**, 1–29.

Garrison, D. L., Gowing, M. M., Hughes, M. P. *et al.* (2000) Microbial food web structure in the Arabian Sea: a US JGOFS study. *Deep-Sea Res. II*, **47**, 1387–1422.

Goericke, R. (2002) Top-down control of phytoplankton biomass and community structure in the monsoonal Arabian Sea. *Limnol. Oceanogr.*, **47**, 1307–1323.

Goericke, R. and Montoya, J. (1998) Estimating the contribution of microalgal taxa to chlorophyll *a* in the field—variations of pigment ratios under nutrient- and light-limited growth. *Mar. Ecol. Prog. Ser.*, **169**, 97–112.

Gordon, L. I., Jennings, J. C., Ross, A. A. *et al.* (1992) A suggested protocol for continuous flow automated analysis of seawater nutrients in the WOCE hydrographic program and the Joint Global Ocean Fluxes Study. Grp. Tech Rpt 92–1, OSU College of Oceanography Descr. Chem. Oc.

Haury, L. R., Venrick, E. L., Fey, C. L. *et al.* (1993) The Ensenada Front: July 1985. *CalCOFI Rep.*, **34**, 69–88.

Holligan, P. M. (1981) Biological implications of fronts on the northwest European continental shelf. *Phil. Trans. R. Soc. Lond.*, **A302**, 547–562.

Hood, R. R., Abbott, M. R. and Huyer, A. (1991) Phytoplankton and photosynthetic light response in the coastal transition zone off northern California in June 1987. *J. Geophys. Res.*, **96**, 14769–14780.

Houghton, R. W. and Marra, J. (1983) Physical/biological structure and exchange across the thermohaline shelf/slope front in the New York Bight. *J. Geophys. Res.*, **88**, 4467–4481.

Jacquet, S., Prieur, L., Avois-Jacquet, C. *et al.* (2002) Short-timescale variability of picophytoplankton abundance and cellular parameters in surface waters of the Alboran Sea (western Mediterranean). *J. Plankton Res.*, **24**, 635–651.

Jeffrey, S. W. and Wright, S. W. (2005) Photosynthetic pigments in marine microalgae. In Subba Rao, D. V. (ed.), *Algal Cultures, Analogues of Blooms and Applications*. Science Publishers, New Hampshire, pp. 33–90.

Kahru, M., Di Lorenzo, E., Manzano-Sarabia, M. *et al.* (2012) Spatial and temporal statistics of sea surface temperature and chlorophyll fronts in the California Current. *J. Plankton Res.*, **34**, 749–760.

Kemp, A. E. S., Pearce, R. B., Grigorov, I. *et al.* (2006) Production of giant marine diatoms and their export at oceanic frontal zones: implications for Si and C flux from stratified oceans. *Global Biogeochem. Cycles*, **20**, GB4S04, doi:10.1029/2006GB002698.

Landry, M. R., Ohman, M. D., Goericke, R. *et al.* (2012) Pelagic community responses to a deep-water frontal system in the California Current Ecosystem: overview of the A-front study. *J. Plankton Res.*, **34**, 739–748.

Lara Lopez, A. L., Davison, P. and Koslow, J. A. (2012) Abundance and community composition of micronekton across a frontal system off Southern California. *J. Plankton Res.*, **34**, 828–848.

Li, Q. P., Franks, P. J. S., Ohman, M. D. *et al.* (2012) Enhanced nitrate fluxes and biological processes at a frontal zone in the southern California Current system. *J. Plankton Res.*, **34**, 790–801.

Monger, B. C. and Landry, M. R. (1993) Flow cytometric analysis of marine bacteria with Hoechst 33342. *Appl. Environ. Microbiol.*, **59**, 905–911.

Ohman, M. D., Powell, J., Picheral, M. *et al.* (2012) Mesozooplankton and particulate matter responses to a deep-water frontal system in the southern California Current System. *J. Plankton Res.*, **34**, 815–827.

Pingree, R. D., Holligan, P. M. and Mardell, G. T. (1978) The effects of vertical stability on phytoplankton distributions in the summer on the northeast European shelf. *Deep-Sea Res.*, **25**, 1011–1028.

Reul, A., Rodríquez, V., Jiménez-Gómez, F. *et al.* (2005) Variability in the spatio-temporal distribution and size-structure of phytoplankton across an upwelling area in the NW-Alboran Sea, (W-Mediterranean). *Cont. Shelf Res.*, **25**, 589–608.

Samo, T. J., Pedler, B. E., Ball, I. G. *et al.* (2012) Microbial distribution and activity across a water mass frontal zone in the California Current Ecosystem. *J. Plankton Res.*, **34**, 802–814.

Schlitzer, R. (2006) Ocean Data View, http://odv.awi.de.

Sherr, E. B. and Sherr, B. F. (1993) Preservation and storage of samples for enumeration of heterotrophic protists. In Kemp, P. K. (ed.), *Handbook of Methods in Aquatic Microbial Ecology*. CRC Press, Boca Raton, FL, pp. 207–212.

Snyder, M. A., Sloan, L. C., Diffenbaugh, N. S. *et al.* (2003) Future climate change and upwelling in the California Current. *Geophys. Res. Lett.*, **30**, doi:10.1029/2003GL017647.

Tangen, K. and Björnland, T. (1981) Observations on pigments and morphology of *Gyrodinium aureolum* Hulburt, a marine dinoflagellate containing 19′-hexanoyloxyfucoxanthin as the main carotenoid. *J. Plankton Res.*, **3**, 389–401.

Taylor, A. G., Landry, M. R., Selph, K. E. *et al.* (2011) Biomass, size structure and depth distributions of the microbial community in the eastern equatorial Pacific. *Deep-Sea Res. II*, **58**, 342–357.

Traganza, E. D., Redalje, D. G. and Garwood, R. W. (1987) Chemical flux, mixed layer entrainment and phytoplankton blooms at upwelling fronts in the California coastal zone. *Cont. Shelf Res.*, **7**, 89–105.

Venrick, E. L. (2000) Summer in the Ensenada Front: the distribution of phytoplankton species, July 1985 and September 1988. *J. Plankton Res.*, **22**, 813–841.